



Study of Comparison Heat Energy Disposal in Hollow Roof Cooling Water Tank using Natural Material

Sudirman Lubis^{1,2}, Farel H. Napitupulu^{1,*}, Ilmi Abdullah¹, Tulus Burhanuddin Sitorus¹, Malik Abdul Karim³

¹ Mechanical Engineering, Faculty of Engineering, Universitas Sumatera Utara, Medan City, Sumatera Utara 20155, Indonesia

² Mechanical Engineering, Faculty of Engineering, Universitas Muhammadiyah Sumatera Utara, Kota Medan, Sumatera Utara 20238, Indonesia

³ Department of Mechanical Engineering, Universiti Teknologi PETRONAS, 32610 Seri Iskandar, Perak, Malaysia

ARTICLE INFO

Article history:

Received 11 March 2024

Received in revised form 22 May 2024

Accepted 10 October 2024

Available online 31 January 2025

Keywords:

Hollow roof; composite; pineapple fibre; fiberglass

ABSTRACT

A cooling tank functions as a heat exchanger utilising water as the working fluid material, while air facilitates water cooling through direct contact, inducing partial water evaporation. The cooled water circulates within the hollow roof, aiming to absorb heat along its path. This paper undertakes a comparative analysis of four roof structures integrating composite layers to discern the most efficient and superior option. The assessment encompasses performance evaluation, thermal insulation properties, environmental resistance, heat absorption capability, energy efficiency, and economic feasibility of the composite layers applied to the roofs. The study aims to determine the effectiveness of the heat transfer rate within the hollow roof, ascertain the hourly energy discharge potential from the cooling water tank, and identify the requisite water flow to supply the hollow roof. Based on the experimentation, Roof 3 exhibited the highest room temperature, followed by Roof 1, Roof 4, and Roof 2. Ultimately, it was observed that Roof 2 possesses a superior ability to absorb heat energy from sunlight compared to other materials.

1. Introduction

Environmental challenges such as climate change and global warming have been exacerbated since the onset of the 21st century, with human activities implicated in over 95% of these issues [1,2]. Many greenhouse gas emissions, notably carbon dioxide, the primary driver of global warming, stem from human activities [3,4]. Particularly noteworthy is the refrigeration sector's contribution of 8% to the global greenhouse gas emissions, imposing significant pressure on ecological equilibrium [5,6]. Cooling solutions, such as compression, adiabatic demagnetisation, laser, and semiconductor, are commonly employed and associated with substantial energy consumption and carbon emissions [7-10].

* Corresponding author.

E-mail address: farel@usu.ac.id

<https://doi.org/10.37934/araset.55.2.1442>

Through transpiring and perspiring water, which boasts one of the highest latent heats among fluids, plants and animals can autonomously adjust to variations in the surrounding environment, such as temperature and relative humidity. Several self-adaptive cooling solutions linked to bio-inspired synthetic skins have been unveiled, encompassing thermochromic reflective coatings and building skins based on superabsorbent polymers, specifically hydrogels. These advancements draw inspiration from the inherent biological cooling mechanisms [11-13]. Hydrogels, while offering promising cooling capabilities, are often less durable than their inorganic counterparts and susceptible to damage from UV radiation and cyclic exposure to moisture and dryness, potentially limiting their long-term viability as building surfaces. To address this, micro-sized fly ash cenospheres (FACs) are incorporated into an inorganic artificial foam through a process involving heating a clay-water solution followed by sintering, resulting in a foam structure characterised by over ninety-five per cent interconnected pores, utilising a technique termed "minimal contact" [14-16]. Consequently, this foam layer can be utilised for prolonged evaporative cooling, aiding in retaining raindrops and facilitating roof waterways [17,18]. Comparative analysis with conventional porous materials and superabsorbent polymers reveals additional benefits of the newly developed material, including its lighter weight and cost-effectiveness [19,20]. Moreover, its composition of sintered inorganic minerals renders it resistant to UV-induced degradation. A biomimetic 'hydro-foam', biomimetic mesoporous synthetic foam (BMSF), is devised as an evaporative cooling layer for building rooftops featuring organised, functional structures. The measured evaporation rate of BMSF flat panels closely resembles that of natural aquatic surfaces, resulting in a substantial cooling effect that minimises air conditioning loads. Integrating BMSF surfaces onto vertical building facades is straightforward and potentially significantly reduces energy consumption for mid-rise and high-rise structures [21].

As technology advances, active cooling systems have become indispensable in urban communities [22]. The utilisation of such systems is steadily increasing, and they currently hold the top position globally. Consequently, there is a growing demand for air conditioning equipment that minimises electricity consumption, with solar energy emerging as a promising alternative power source [23,24]. Passive cooling systems, albeit unable to match the performance of active counterparts, are being explored by researchers, offering potential energy savings during summer months by deflecting solar radiation away from structures into space [25,26]. Composite materials comprising natural and synthetic fibre blends [27-29] are also being considered for roofing applications in various studies, focusing on optimising thermal conductivity to function akin to solar collectors, directly absorbing heat energy from sunlight. Rui *et al.*, [30] investigated room coverings using composite materials to mitigate temperature fluctuations indoors, aiming to enhance overall comfort levels. Rui introduced sodium acetate into the composite mixture, along with trihydrate (SAT) and formamide (FA) combined with expanded perlite (EP) to impart new physical properties to the composite material. Similarly, Chang *et al.*, [31] researched optimising energy efficiency within enclosed spaces by employing a roof constructed from three overlaid materials: plastic, wood, and composite. In another study, Ghosh *et al.*, [32] conducted a failure analysis on composite layers used in residential roofs in Indian communities, exploring three fibre variations: sloping, angular, and cross. Their findings indicate that the inclined fibre layer outperforms the angled and cross-fibre configurations, highlighting its structural integrity and performance superiority.

Research on the mechanical properties of composite roofing materials remains ongoing, with advancements in laminated configurations being explored. Neogi *et al.*, [33] conducted a study involving finite element analysis of layered roof structures in an inclined state with slight friction applied. In another investigation, Irawati *et al.*, [34] developed a wooden composite roof supplemented with a laminated layer of wood composite. The findings indicate that the laminated

wood roof outperforms conventional wooden roof frames withstanding external loads. In Malaysia, K.S. Ong [35] conducted an experiment involving six rooms, each equipped with different roofing materials, with dimensions of 2 meters in length and 1 meter in width. The roofs were inclined at a 15-degree angle, with variations in materials, including metal roofing, concrete roofs, and roofs featuring heat insulation layers such as aluminium foil, coupled with provisions for adequate air circulation. Data was collected at 5-minute intervals over 24 hours for several weeks, enabling a comparison of roof temperatures across the six roof types. At midday, the roof temperature of the uninsulated model ranged from 40°C to 50°C, exceeding ambient temperatures by up to 10°C, while at night, the temperature was one °C lower than the environment. The second model, with insulation beneath the tiles, exhibited attic temperatures ranging from 30°C to 40°C, with the temperature behind the attic sidewall being three °C lower. Due to their higher thermal mass, metal deck roof designs demonstrated more significant temperature fluctuations than standard concrete roof designs. Each roof exhibited a transient thermal response, with standard roofs displaying the slowest response to solar radiation. Due to increased heat absorption, standard tiles recorded the lowest roof temperatures among tile roof designs. The study revealed that metal roofs with insulation underneath exhibited the highest roof temperatures, suggesting that insulation beneath tiles is preferable to insulation above the ceiling.

Tile roofs with insulation underneath exhibit elevated temperatures due to limited heat dissipation to both the external environment and the lower side of the attic. In Istanbul, Turkey, Khalifa [36] conducted a study focusing on the cooling effect of rooftop ponds on buildings, assessing both energy and exergy considerations. The findings revealed that implementing rooftop pools can lower room temperatures by a minimum of 4°C compared to conventional roofs. With solar intensity peaking at 3500 kJ/hr.m², the maximum temperature recorded in a room with a pond roof was 37°C, representing a 42°C difference from rooms without such roofing systems, with the average ambient temperature at that time being 43.5°C. Meanwhile, in Tianjin, China, Kong *et al.*, [37] investigated phase change material (PCM) roofing materials to reduce building energy absorption and enhance room comfort by augmenting thermal storage capacity. Two PCM systems, PCMOW (capric acid incorporated into panels installed externally) and PCMIW (capric acid and 1-dodecanol within panels installed internally), were numerically developed. Three rooms measuring 2m × 2m × 2.4m were constructed to evaluate the performance of the PCM panel system. Under free cooling conditions, the inner surface temperature of the roofs in PCMOW and PCMIW rooms was lower than that of spaces lacking PCM. The temperature of a standard roof reached 45°C, exceeding that of roofs incorporating PCM, which maintained an average temperature of 30°C. This underscores the efficacy of PCM in mitigating heat transfer into indoor spaces.

Kumar *et al.*, [38] investigated roof cooling mechanisms involving insulation, concluding that effective insulation significantly hampers heat transfer processes, reducing roof heat conductivity. Commonly employed insulating materials include polystyrene combined with polyurethane foam, concrete foam, fiberglass, styropor, peripor, and neopor. Without insulation, roof temperatures typically range from 42°C to 48°C, facilitating heat transfer into the interior space. Following insulation application, an average temperature difference of 4.8°C was observed compared to uninsulated conditions within the room. In a related study, Al-Obaidi *et al.*, [39] explored passive cooling systems on building roofs, employing reflective methods to mitigate heat buildup and redirect solar radiation away from the structure. Roof colouring techniques aim to reduce the heat conductivity of roofing materials, which is particularly prevalent in lightweight metal roofs known for their high thermal conductivity. The study concluded that white colouring effectively reduces heat absorption, enhancing cooling efficiency.

2. Material and Methods

2.1 Material

This prototype aims to regulate room temperature, ensuring excellent thermal stability. The roofing material was fabricated using glass fibre, wood fibre, and rice husk fibre combined with resin 801, mimicking the undulating profile of conventional steel roofs. Four prototype rooms were constructed, each measuring 1 x 1 x 1 meter with a wall thickness of approximately 15 cm. These rooms featured roofs composed of distinct composite materials, designated as R1, R2, R3, and R4, comprising rice husk and pineapple, rice husk and wood fibre, zinc and rice husk, and glass fibre, respectively. A cavity was incorporated into the centre of each roof to facilitate the flow of cooling water sourced from a tank. Each roof had ten cavities, each holding approximately 0.0064 m³ of water. A DC pump rated at 12 V and 10 Watts, with a current draw of 0.8 A, capable of operating within a temperature range of 2-110°C and achieving a maximum volume flow rate of 8 litres per minute, was utilised. The pump featured inlet and outlet ports measuring 1/4 inch in diameter. Furthermore, a single-piece 100 Wp solar panel with an automatic charging system was employed. Measurement instrumentation included an anemometer, pyranometer, K-type thermometer, and thermocouple to assess ambient wind speed, solar irradiance, environmental temperature, and temperature at predetermined points within each room, respectively. Agilent temperature measuring instruments were employed to record data from thermocouples, resistance temperature detectors (RTDs), and AC electric currents at five-minute intervals, as illustrated in Figure 1.

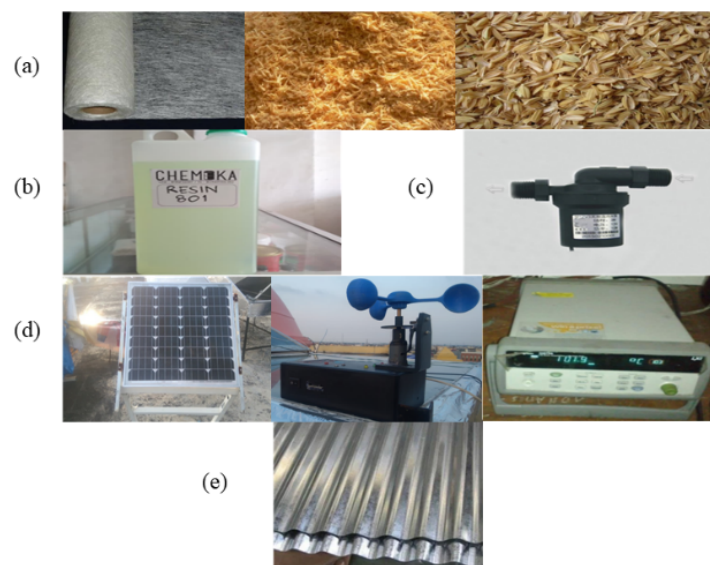


Fig. 1. (a) Glass fibre, wood fibre and rice husk fibre (b) resin 801 (c) electric pump (d) solar panels, anemometer, Agilent temperature measuring instrument (e) zinc roof

The intensity of solar radiation is a critical factor influencing temperature variations. Sensors were strategically positioned at approximately seven predefined locations within each prototype room. Data collection spanned seven days, with observations conducted over approximately 10 hours each day. Data collection commenced in the morning at approximately 08:00 WIB (Western Indonesian Time) and concluded at 17:00.

2.1 Mathematical Model

During the experimentation phase, various heat transfer phenomena within the system were analysed to quantify the energy absorbed when solar radiation strikes the roof surface, evaluate the effectiveness of the roof cooling apparatus, and assess temperature differentials between rooms equipped with cooling roofs versus conventional roofs. The heat transfer processes occurring on the roof were elucidated. Figure 2 illustrates a segment of the heat transfer process on a conventional roof devoid of interior and exterior cooling mechanisms.

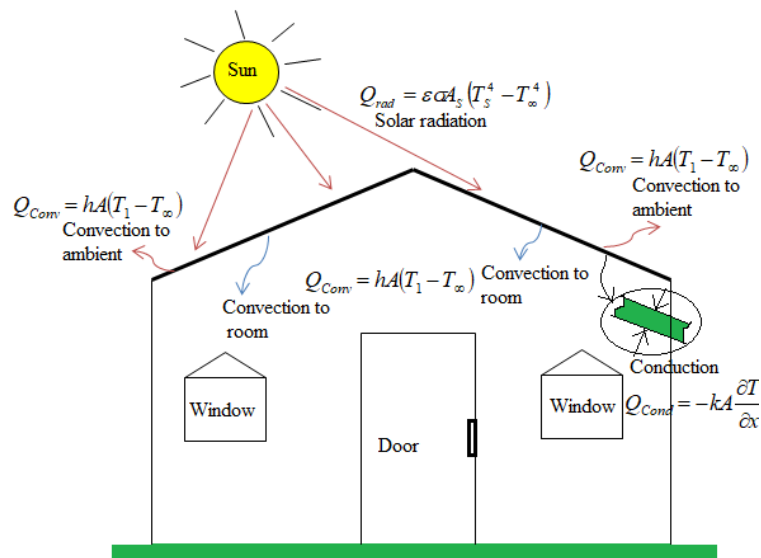


Fig. 2. Schematic of the heat transfer process in a room with a conventional roof

In contrast, Figure 3 delineates the operational principle of the undulating cooling roof and illustrates the heterogeneous heat transfer processes occurring across the roof surface, influenced by environmental factors intersecting with the roof.

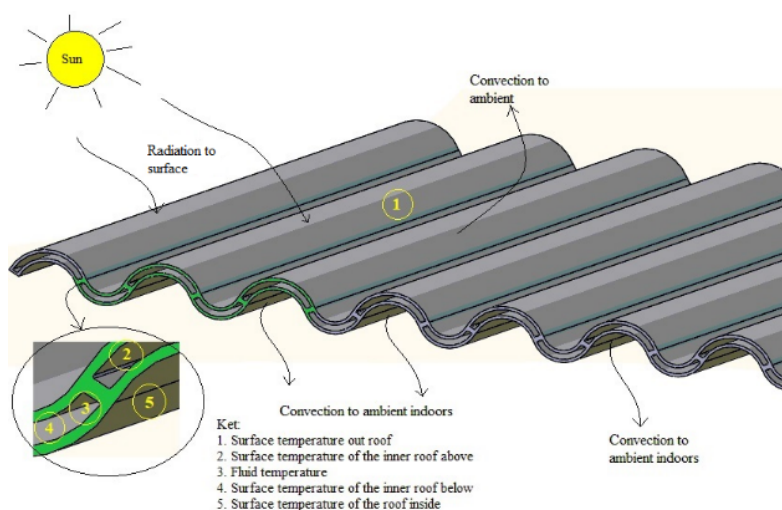


Fig. 3. Prototype wave cooling roof with heat transfer points

2.2.1 Radian heat transfer on the roof

The roof surface is directly exposed to sunlight, initiating a radiation process. Solar thermal energy is absorbed by the roof surface and subsequently conducted into the roofing material. The quantity of energy absorbed is quantified by positioning a heat sensor on the roof surface, enabling the measurement of surface temperature and, consequently, the energy absorbed per hour. The fundamental equation governing radiation, derived from Fourier's law, is represented by Eq. (1) [40].

$$Q_{rad} = \epsilon \sigma A_s (T_s^4 - T_\infty^4) \quad (1)$$

The operational principle of the cooling roof parallels that of a flat plate collector, wherein solar energy is captured and transferred to a fluid medium [41,42]. However, unlike traditional solar collectors employing metal plates with high thermal conductivity, cooling roofs utilise composite materials with low thermal conductivity. The total radiant heat energy absorbed is computed using Eq. (2) [43-46].

$$Q_{rad} = \frac{\epsilon_g \times \sigma \times (T_1^4 - T_{sky}^4)}{(T_1 - T_a)} \quad (2)$$

Where the value of air temperature was used by Eq. (3) [47]

$$T_{sky} = T_a - 6 \quad (3)$$

2.2.2 Convection of the roof surface into the environment and deep crushing into the fluid

Due to the energy absorbed by the roof via radiation heat transfer from its outer surface, a reduction in energy loss was observed due to the convection heat transfer process between the roof surface and the surrounding environment. This reduction in energy loss was crucial to prevent excessive thermal energy from penetrating the interior space. To assess the fluid's capacity to absorb heat from the sun-exposed roof surface, calculations were conducted to determine the magnitude of heat transfer between the outer surface and the environment and between the inner surface and the fluid. Fourier's law governing convection heat transfer was utilised for these calculations, as expressed in Eq. (4) [40].

$$Q_{Conv} = hA(T_s - T_\infty) \quad (4)$$

The energy dissipated into the surrounding air and absorbed by the coolant served to mitigate the amount of solar energy absorbed by the roof, resulting in a beneficial reduction in thermal energy on the outer roof surface facilitated by convective airflow. The heat transfer coefficient (h) in Equation 4 represents heat transfer effectiveness from the roof to the surrounding air, and its value was derived from Eq. (5) [45,48].

$$h_{C\infty} = \begin{cases} [5.7 + 3.8 \times V] \leq 5 \text{ m/s} \\ [6.15 \times V^{0.8}] > 5 \text{ m/s} \end{cases} \quad (5)$$

The magnitude of wind speed in the outdoor environment significantly influences the convection heat transfer coefficient between the roof and the surroundings. Therefore, wind speed data was crucial during experimentation and was recorded using anemometer sensors. Meanwhile, the heat transfer coefficient value for water was determined by considering the physical properties of water, as detailed in Table 1.

Table 1

Physical properties of water at 1 atm

Temperature (°C)	Density (Kg/m ³)	Specific Heat (kJ/kg K)	Boiling Point (°C)	Latin Heat of vaporisation (kJ/kg)
0	1000	4,22	100	2257

A cooling fluid flow was planned for an electric pump, and the convection heat transfer equation was applied. To calculate the value of the coefficient of heat transfer of water in the roof pore Eq. (6) [49].

$$h_f = \frac{N_u \times k}{D_h} \quad (6)$$

D_h is the hydraulic diameter depending on the shape of the diameter or geometry of the flow cross-section, and N_{you} is the dimensionless number [40].

$$N_u = \frac{hL}{k} \quad (7)$$

The loss of pressure on the inlet and outlet due to fluid friction into the roof wall is shown in Eq. (8) [40].

$$W_{pump} = \dot{Vol} \times \Delta P \quad (8)$$

where Vol is the flow rate of the volume of water in the pore of the cooling roof (m³/s), was calculated in Eq. (10) [50].

$$V_f = \frac{\dot{m}}{A \times \rho_f \times \int \frac{w_2}{w}} \quad (10)$$

So, Eq. (9) obtained the value of the average convection coefficient of the cooling fluid as shown in Eq. (11) [50].

$$h_f = \left(1430 + 23,3(T_{f,m} - 273,15) - 0,048(T_{f,m} - 273,15)^2\right) v_f^{0,8} A_i^{-0,2} \quad (11)$$

The heat that moved from the outer surface of the roof was conducted into the roof and transferred to the cooling fluid flowing inside the roof. The amount of energy that transferred conductively from the surface to the cooling fluid was calculated by knowing the thermal conductivity value of the roofing material composite.

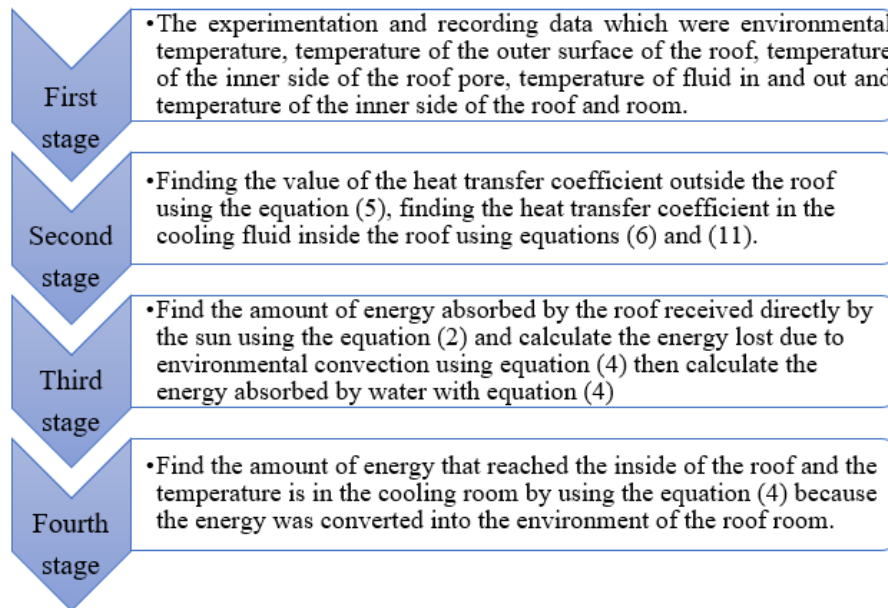


Fig. 5. Steps for analysing data

3. Results and Discussion

3.1 Solar Intensities Data

Solar intensity emerges as a pivotal variable in this investigation, directly impacting the temperature absorbed by the roof. Figure 6 delineates the temporal distribution of solar intensity, revealing a peak occurrence on the sixth day between 10:00 and 11:00 WIB, with an average intensity nearing 900 W/m². Data collection exhibited occasional gaps attributed to various factors, including natural occurrences like rainfall and potential human errors such as oversight during temperature sensor installation. Days with diminished solar intensity, notably the fifth and seventh days, experienced periods where solar intensity levels nearly reached zero W/m². Conversely, solar intensity remained relatively stable on other days, averaging between 100 and 600 W/m².

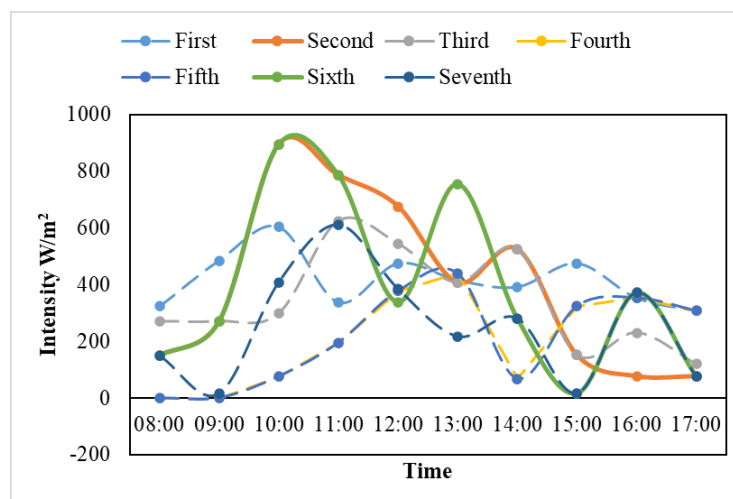


Fig. 6. Solar intensities of seven days

3.2 Wind Velocity Data

Wind velocity emerges as a crucial variable in this study, influencing atmospheric pressure exerted on the roof as air moves from areas of high to low pressure. Figure 7 illustrates the temporal variation of wind velocity, revealing peak values of 23 m/s observed on the second, third, fifth, and sixth days at 9:00, 11:00, 12:00, 15:00, and 16:00 WIB, respectively. However, data collection was subject to natural factors such as rainfall and potential human errors. Some days, they exhibited lower wind velocities, notably on the first day, where wind velocity consistently hovered around five m/s throughout the observation period. Conversely, wind velocity remained relatively stable on other days, averaging between 5 and 20 m/s.

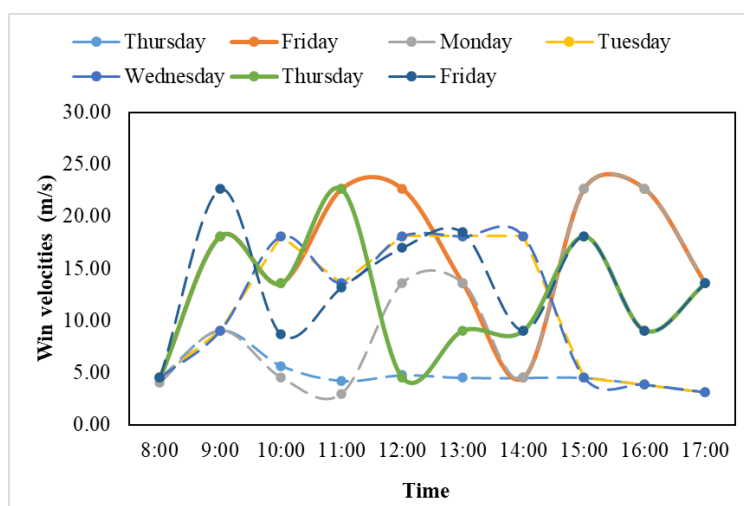


Fig. 7. Wind velocities of seven days

3.3 Ambient Temperature

Ambient temperature serves as a pivotal variable in this study, directly influenced by solar intensity and impacting the thermal conditions experienced by the roof. Figure 8 presents the ambient temperature data collected for all four roofs over seven days. Figures 8 (b), (c), (d), (f), and (g) display the ambient temperature trends for each roof on the second, third, fourth, sixth, and seventh days, respectively. The peak ambient temperatures, ranging from 30-35°C, were typically observed between 8:00 and 9:00 WIB, while the lowest peaks, ranging from 20-25°C, were recorded between 11:00 and 12:00 WIB across the observation period. However, variations in ambient temperature levels were evident on certain days, as illustrated in Figures 8 (a) and (e). These days, peak temperatures also range from 30-35°C at 8:00 to 9:00 WIB, with lowest peaks recorded between 20-25°C at 11:00 to 12:00 WIB.

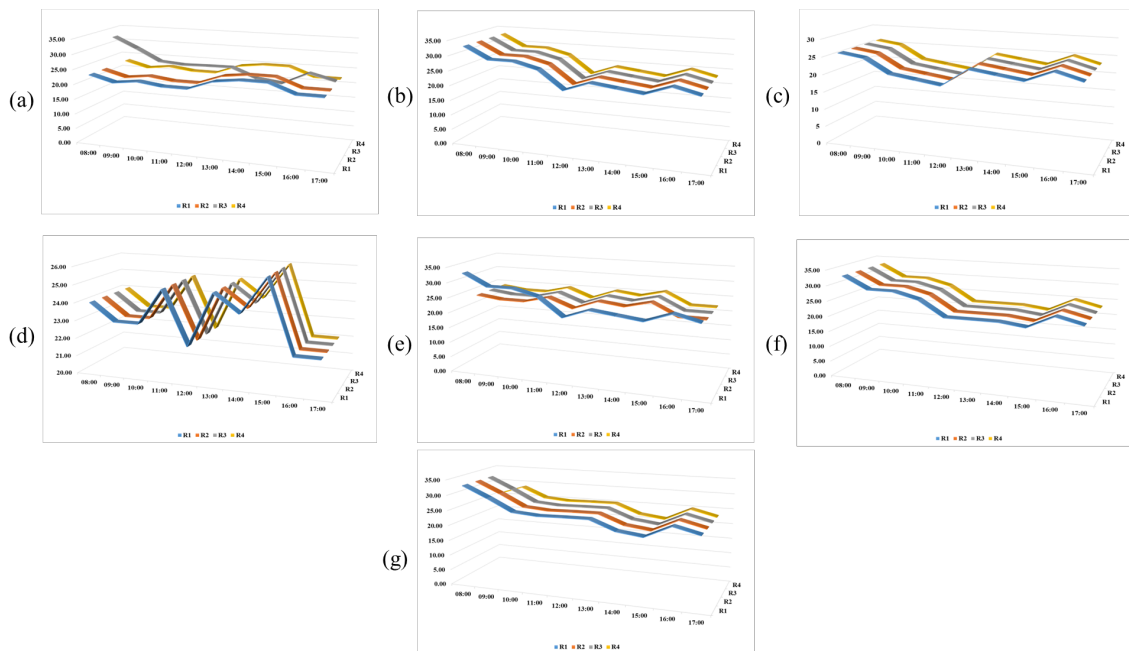


Fig. 8. Total ambient temperatures of all house roofs

3.4 Relative Humidity

Relative humidity is a significant factor in this study, inversely impacting both solar intensity and ambient temperature received by the roof. Figure 9 depicts the relative humidity data collected for all four roofs over seven days. The graph displays consistent relative humidity trends for each roof across all seven days. The highest relative humidity, reaching 90%, was typically recorded at 8:00 WIB, while the lowest relative humidity levels, ranging from 0% to 30%, were observed between 9:00 and 12:00 WIB throughout the observation period.

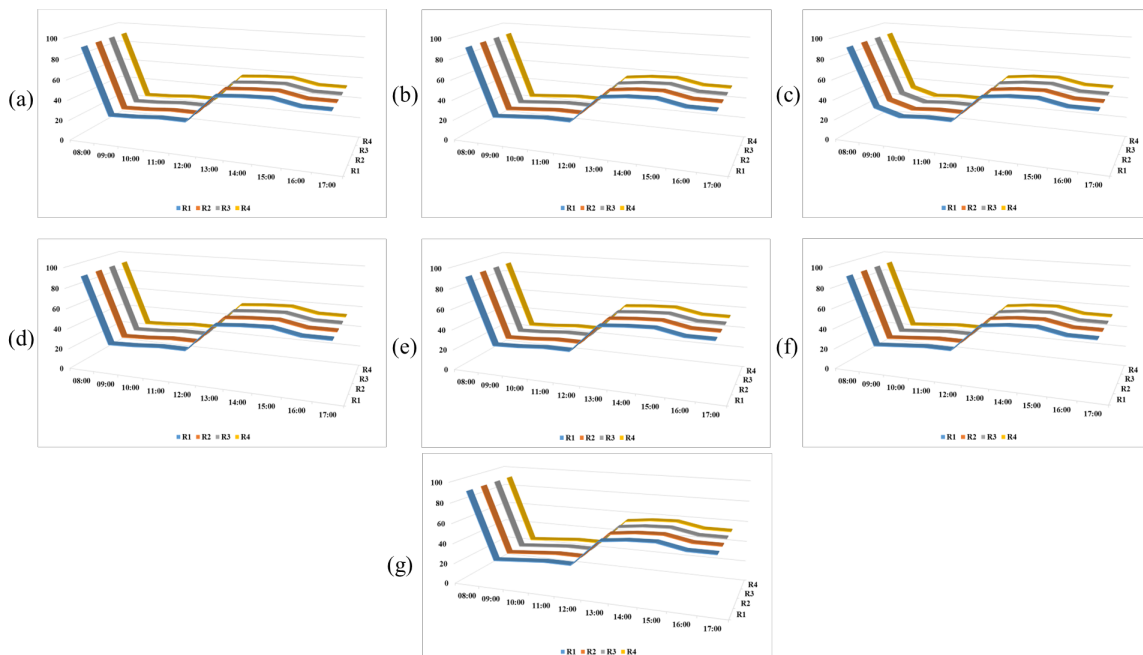


Fig. 9. Relative humidity of all house roofs

3.5 House 1 (Rice Husk and Pineapple Material)

3.5.1 Heat temperature data

Figure 10 illustrates the temperature variations observed over seven days, encompassing water, inner and outer roof, and ambient temperatures. Each subfigure (a-g) corresponds to a specific day of observation. Figure 10 (a) details the temperature profile for day one, commencing from 20°C, representing the lowest temperature of water entering the roof. The highest temperature recorded was 80°C, observed within the water on the western side roof. Figure 10 (b) outlines the temperature trends for day two, with a similar starting temperature of 20°C for water entering the roof. The highest temperature reached 60°C, noted within the water on the eastern side roof. Day three, depicted in Figure 10 (c), commenced with water entering the roof at 20°C. The highest temperature recorded was 55°C, observed within the water on the western side roof. Figure 10 (d) illustrates the temperature variations observed on day four, with a starting temperature of 20°C for water entering the roof. The highest temperature recorded was 80°C, observed within the water on the western side roof. Day five, represented in Figure 10 (e), featured a starting temperature of 20°C for water entering the roof. The highest temperature reached 90°C, noted within the water on the eastern side roof. Figure 10 (f) depicts the temperature fluctuations observed on day six, with a starting temperature of 20°C for water entering the roof. The highest temperature recorded was 70°C, observed within the water on the eastern side roof. Lastly, Figure 10 (g) outlines the temperature dynamics observed on day seven, with ambient and water entering the roof registering the lowest temperatures. The highest temperature recorded was 90°C, observed within the water on the western side roof.

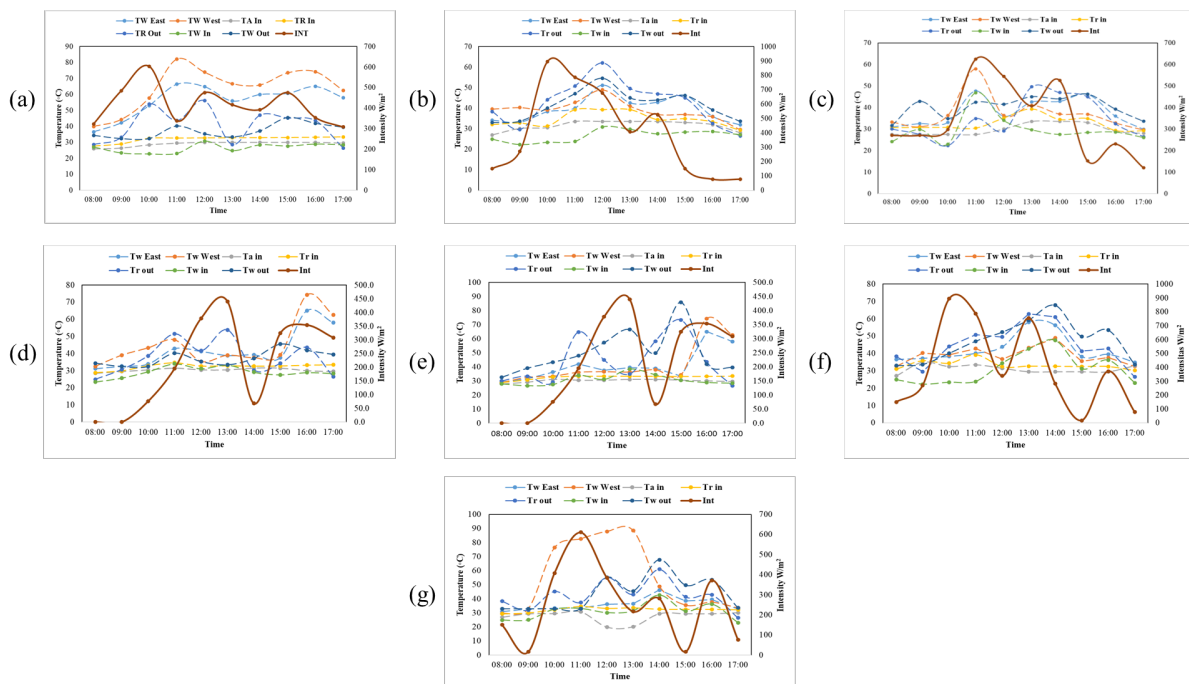


Fig. 10. The temperature data

Here,

- Tw east = Water temperature inside the roof on the east side.
- Tw west = Water temperature inside the roof on the west side.
- Ta in = Ambient temperature inside.
- Tr in = Inner roof surface temperature (east and west).
- Tr out = Outside roof surface temperature (east and west).

$T_{w\ in}$ = Water temperature entering the roof.
 $T_{w\ out}$ = Water temperature coming out of the roof

3.5.2 Heat transfer rate

Figure 11 presents the inner and outer roof surface temperatures and the total heat observed over seven days. The graph illustrates fluctuations in energy levels detected by the sensor, with the highest peak reaching 150 J/s at 15:00 WIB on the fifth day and the lowest point dipping to approximately -20 J/s at 17:00 WIB. Regarding temperatures, the outer roof temperatures (both east and west) consistently exceed those of the inner roof, ranging between 60°C to 70°C. In contrast, the inner roof temperature remains relatively stable, ranging between 25°C to 35°C throughout the observation period.

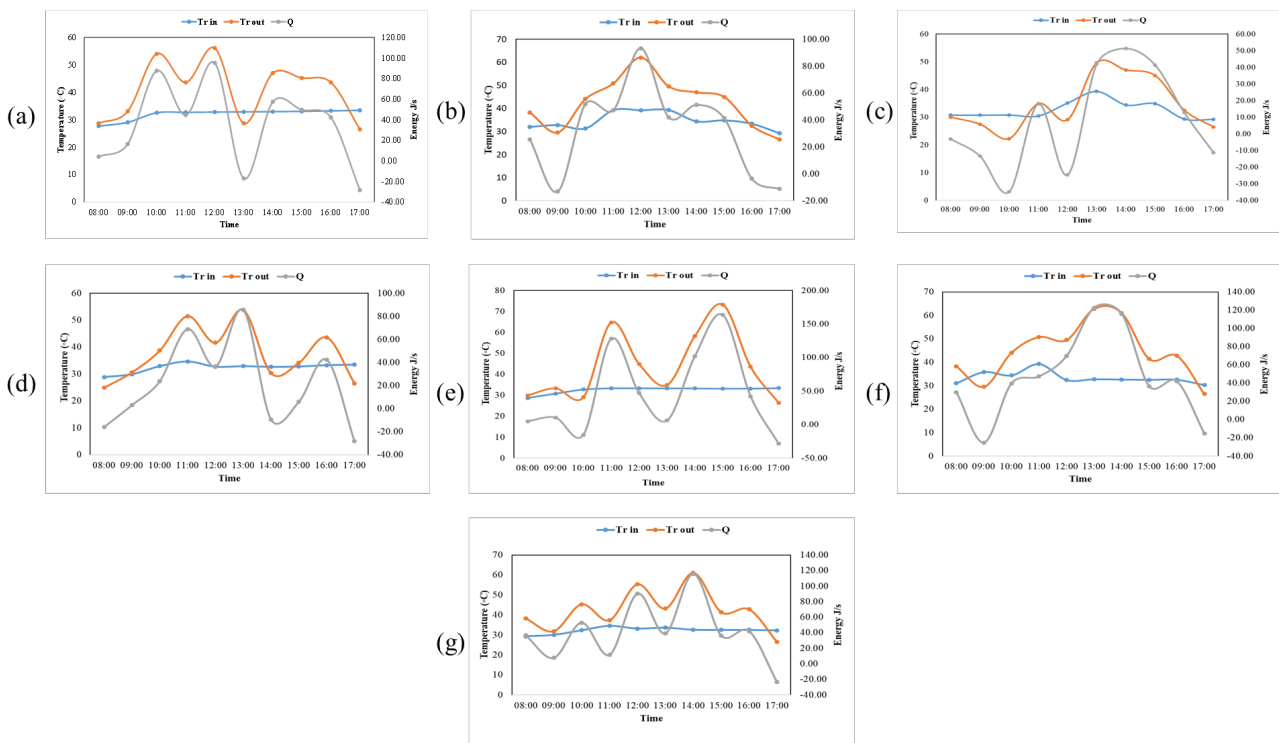


Fig. 11. Conduction

Here,

$T_{r\ in}$ = Inner roof surface temperature (east and west).

$T_{r\ out}$ = Outside roof surface temperature (east and west).

Q = Total heat

3.5.2 Convection

Figure 12 illustrates various temperature parameters observed over the seven-day duration, including water temperatures within the roof on both eastern and western sides, water temperature upon entering the roof, and heat levels on the eastern and western sides of the roof. Throughout the observation period, the heat on the western side consistently remains lower than on the eastern side of the roof, remaining below 40 J/s. Conversely, on the fifth day, the heat on the eastern side peaks at 250 J/s between 15:00 and 16:00 WIB. Regarding water temperatures, the temperature of water

entering the roof consistently registers the lowest values, ranging between 30°C to 40°C, compared to the internal roof temperatures on both the eastern and western sides. Additionally, the temperature on the western side exhibits a notable spike, reaching a value of 90 from 12:00 to 13:00 on the last day of observation.

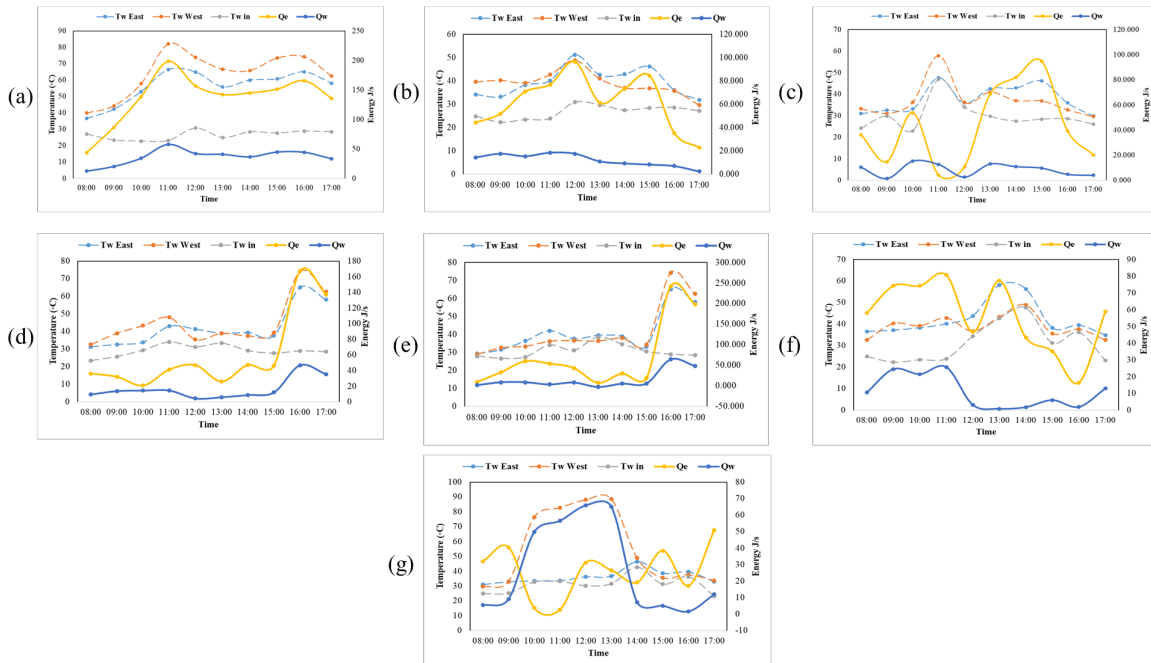


Fig. 12. Convection

Here,

Tw east = Water temperature inside the roof on the east side.

Tw west = Water temperature inside the roof on the west side.

Tw in = Water temperature entering the roof.

Qe = Heat on the east.

Qw = Heat on west

3.5.3 Radiation

Figure 13 presents the water temperature within the roof, ambient temperature, and total heat over the seven days. The chart indicates that the highest energy detected by the sensor peaked at 1.2 J/s at 15:00 WIB on the fifth day, while the lowest point was approximately 0 J/s at 17:00 WIB. The water temperature consistently exceeds the ambient temperature, ranging between 50°C to 70°C. In contrast, the ambient temperature remains relatively stable, ranging between 10°C to 30°C throughout the observation period.

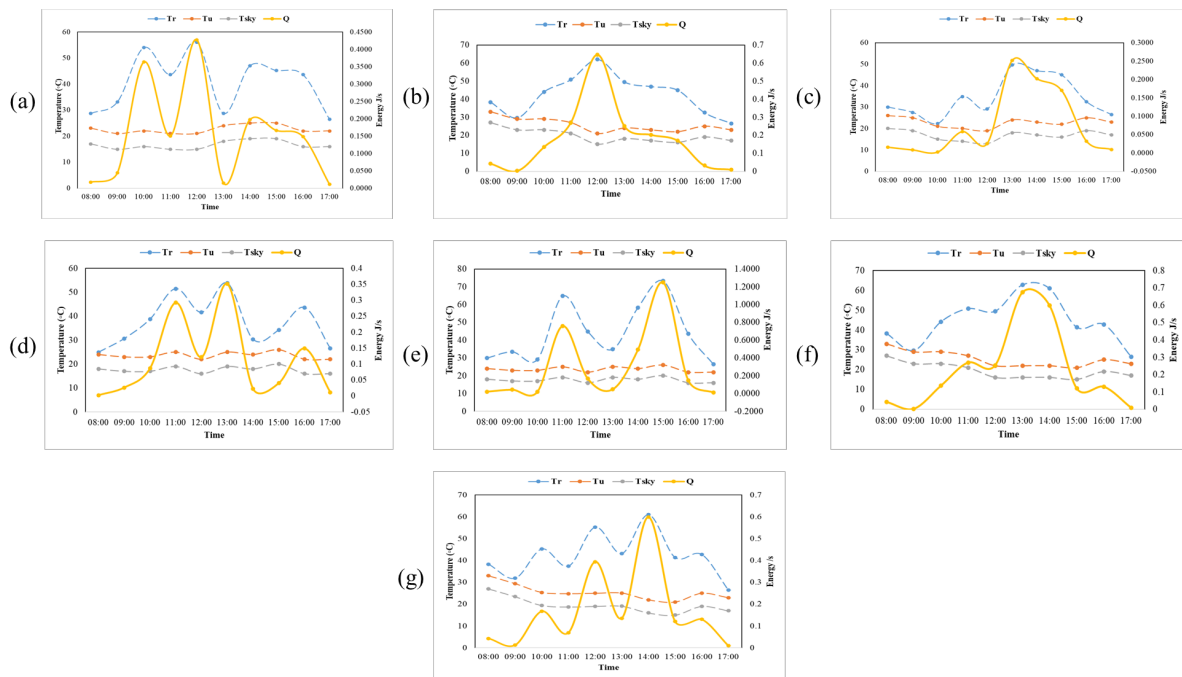


Fig. 13. Radiation

Here,

Tr = Water temperature inside the roof.

T_{sky} = Ambient temperature.

Q = Total heat

3.6 House 2 (Rice Husk and Wood Fibre Material)

3.6.1 Heat temperature data

Figure 14 depicts various temperature parameters observed over seven days, including water, inner and outer roof, and ambient temperatures. The temperature range started from 20°C, representing the lowest recorded water temperature entering the roof. The highest temperature recorded was 120°C, observed within the water on both the eastern and western sides of the roof.

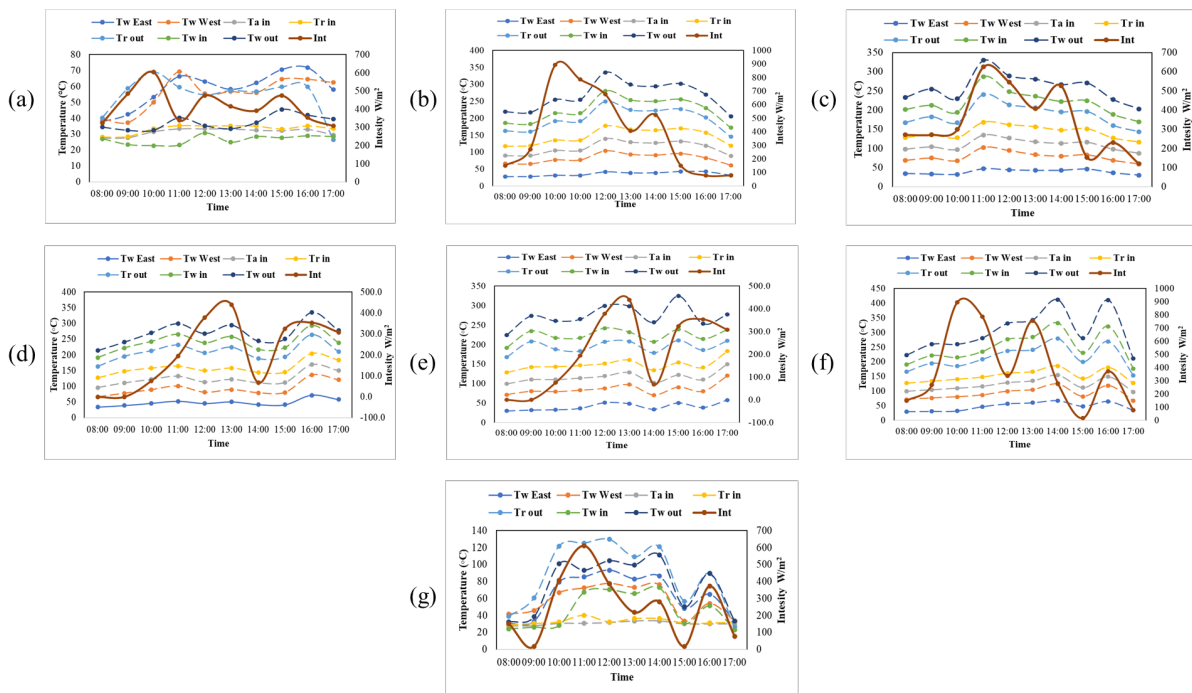


Fig. 14. The temperature data

Here,

Tw east = Water temperature inside the roof on the east side.

Tw west = Water temperature inside the roof on the west side.

Ta in = Room temperature inside.

Tr in = Inner roof surface temperature (east and west).

Tr out = Outside roof surface temperature (east and west).

Tw in = Water temperature entering the roof.

Tw out = Water temperature coming out of the roof.

3.6.2.1 Conduction

Figure 15 illustrates the inner and outer roof surface temperatures and the total heat observed over seven days. The chart indicates that the highest energy detected by the sensor peaked at 400 J/s at noon WIB on the last day, while the lowest value was approximately -40 J/s at 17:00 WIB. Regarding temperatures, the outer roof temperatures (both east and west) consistently surpass those of the inner roof, ranging between 70°C to 130°C. Conversely, the inner roof temperature remains relatively stable, ranging between 25°C to 35°C throughout the observation period.

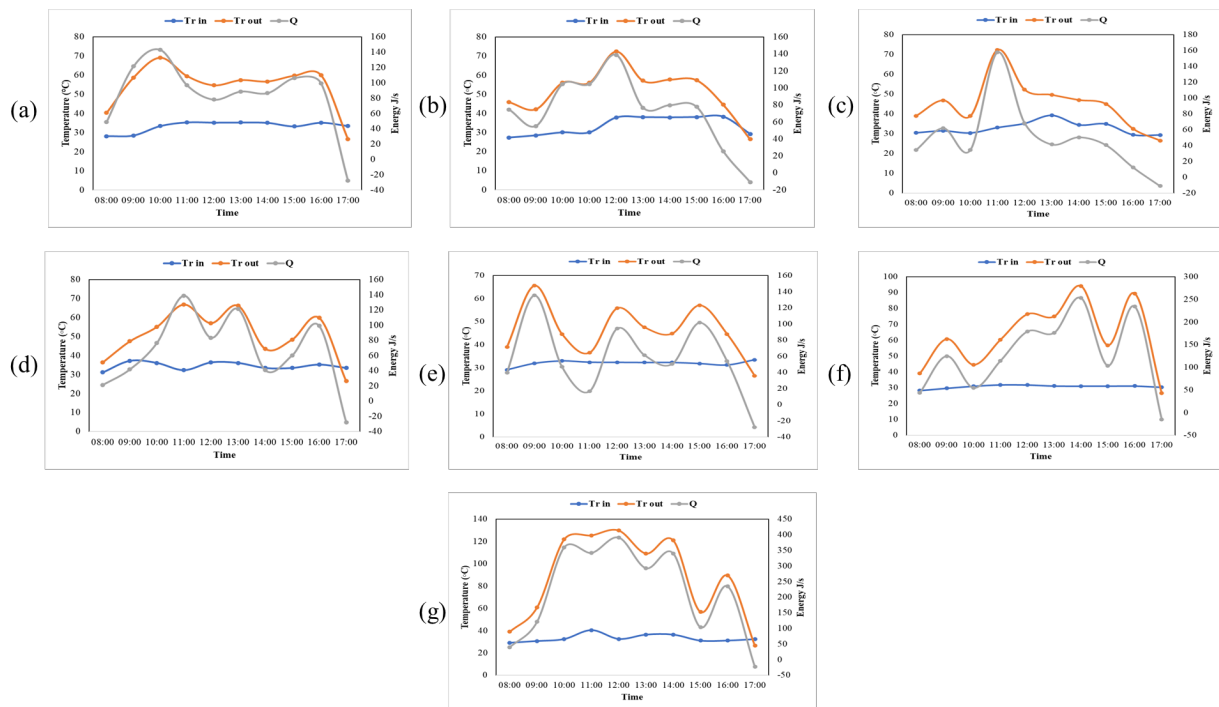


Fig. 15. Conduction

Here,

Tr in = Inner roof surface temperature (east and west).

Tr out = Outside roof surface temperature (east and west).

Q = Total heat

3.6.2.2 Convection

Figure 16 presents the various temperatures recorded over the seven days, including water temperatures within the roof on the eastern and western sides, water temperature upon entering the roof, and heat levels on the eastern and western sides of the roof. Throughout the observation period, the heat on the western side consistently remains lower than that on the eastern side of the roof, consistently below 20 J/s. However, on the last day, the heat on the eastern side peaked at 250 J/s at 10:00 WIB. Regarding water temperatures, the temperature upon entering the roof generally ranged between 20°C to 40°C, except on the last day when it reached 60°C to 70°C between 10:00 and 15:00 WIB. Meanwhile, the temperature inside the roof on both the eastern and western sides consistently remained higher, reaching 70°C. Additionally, the temperature on the eastern side peaked at 90 at noon on the last day.

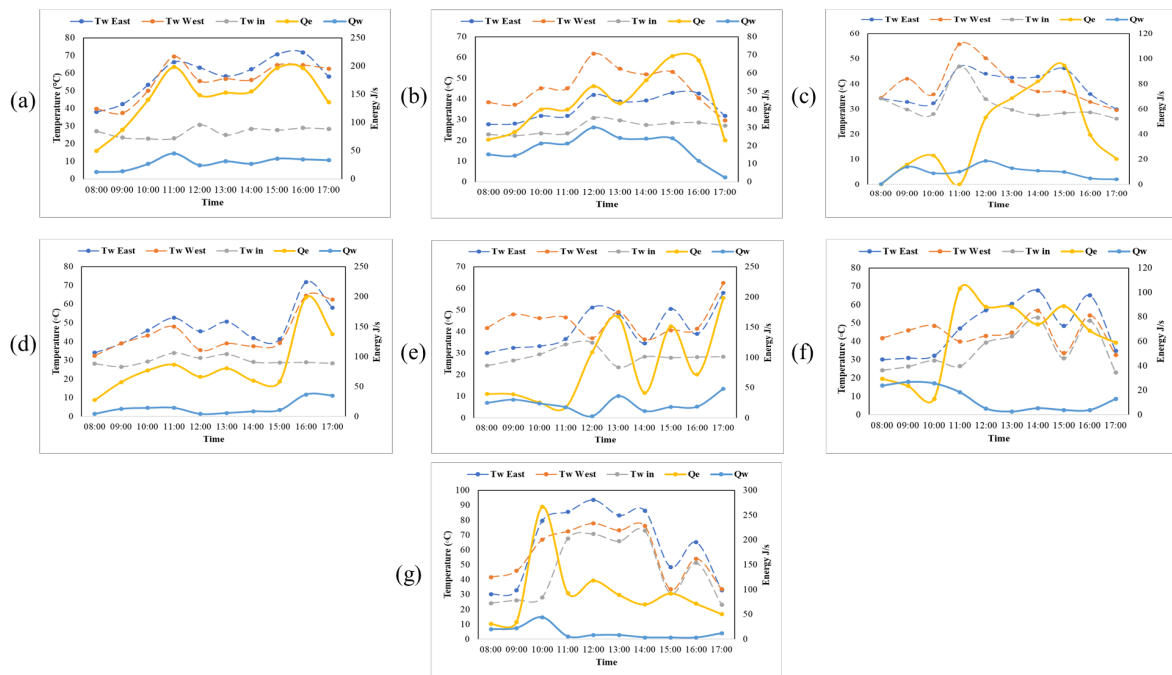


Fig. 16. Convection

Here,

Tw east = Water temperature inside the roof on the east side.

Tw west = Water temperature inside the roof on the west side.

Tw in = Water temperature entering the roof.

Qe = Heat on the east.

Qw = Heat on west

3.6.2.3 Radiation

Figure 17 illustrates the water temperature within the roof, ambient temperature, and total heat observed over seven days. The chart indicates that the highest energy detected by the sensor peaked at 12 J/s at noon WIB on the last day, while the lowest value was approximately 0 J/s at 17:00 WIB. The water temperature consistently exceeds the ambient temperature of 40°C to 120°C. In contrast, the ambient temperature remains relatively stable, ranging between 20°C to 30°C throughout the observation period.

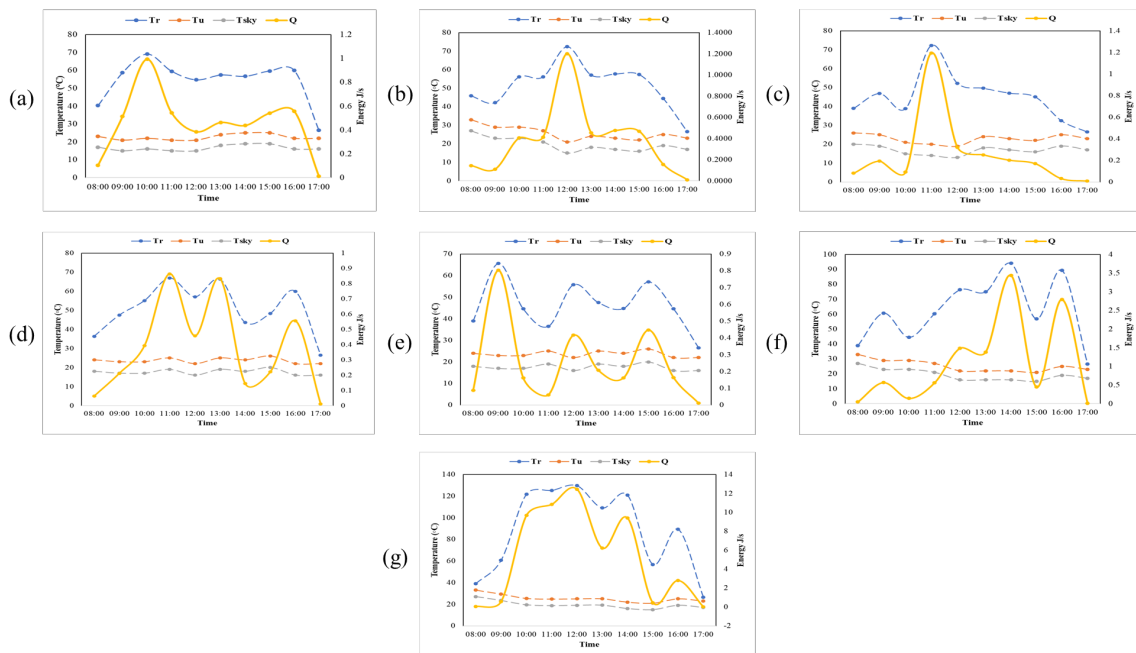


Fig. 17. Radiation

Here,

Tr = Water temperature inside the roof.

T_{sky} = Ambient temperature.

Q = Total heat

3.7 House 3 (Zinc)

3.7.1 Heat temperature data

Figure 18 displays the various temperatures recorded over the seven-day period, including water, inner and outer roof, and ambient temperatures. The temperature range began at 20°C, representing the lowest recorded water temperature entering the roof. The highest temperature recorded was 120°C, observed within the water on both the eastern and western sides of the roof.

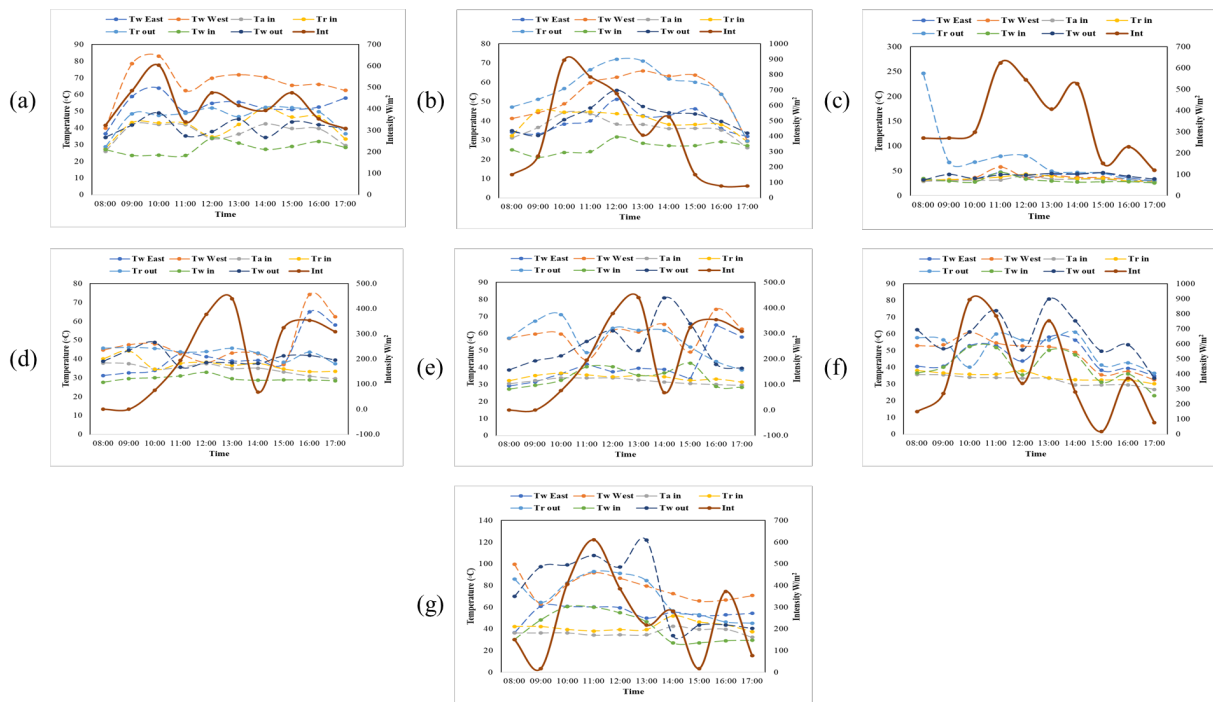


Fig. 18. The temperature data

Here,

- Tw east = Water temperature inside the roof on the east side.
- Tw west = Water temperature inside the roof on the west side.
- Ta in = Room temperature inside.
- Tr in = Inner roof surface temperature (east and west).
- Tr out = Outside roof surface temperature (east and west).
- Tw in = Water temperature entering the roof.
- Tw out = Water temperature coming out of the roof.

3.7.2. Heat transfer rate

3.7.2.1 Conduction

Figure 19 illustrates the inner and outer roof surface temperatures and the total heat observed over seven days. The chart indicates that the highest energy detected by the sensor peaked at 4000 J/s between 10:00 and 11:00 WIB on the last day, while the lowest value was approximately 0 J/s at 17:00 WIB. Regarding temperatures, the outer roof temperatures (both east and west) consistently exceed those of the inner roof, ranging between 70°C to 80°C. Conversely, the inner roof temperature remains relatively stable, ranging between 30°C to 45°C throughout the observation period.

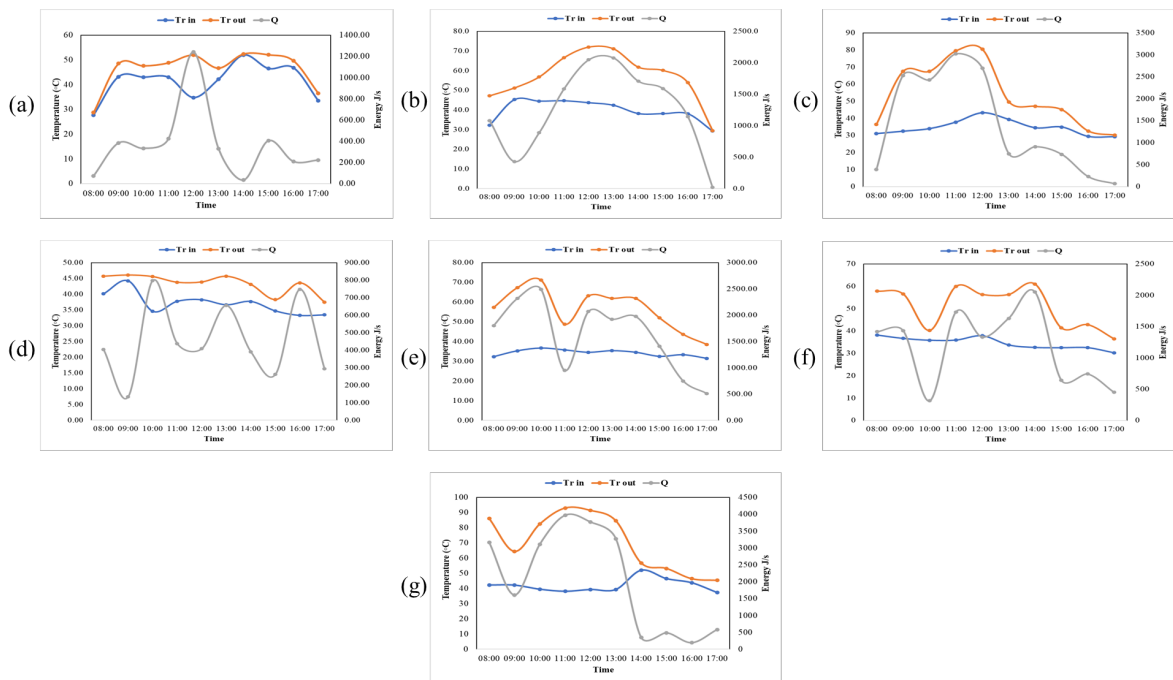


Fig. 19. Conduction

Here,

Tr in = Inner roof surface temperature (east and west).

Tr out = Outside roof surface temperature (east and west).

Q = Total heat.

3.7.2.2 Convection

Figure 20 presents the various temperatures recorded over the seven days, including water temperatures within the roof on the eastern and western sides, water temperature upon entering the roof, and heat levels on the eastern and western sides of the roof. Throughout the observation period, the heat on the western side consistently remains lower than on the eastern side of the roof, consistently below 50 J/s. However, on the fifth day, the heat on the eastern side peaked at 250 J/s at 16:00 WIB. Regarding water temperatures, the temperature upon entering the roof generally ranged between 20°C to 40°C, except on the sixth and seventh days when it reached 50°C to 60°C between 10:00 to 11:00 WIB. Meanwhile, the temperature inside the roof on both the eastern and western sides consistently remained higher, reaching 70°C. Additionally, the temperature on the western side peaked at 100 at 8:00 on the last day.

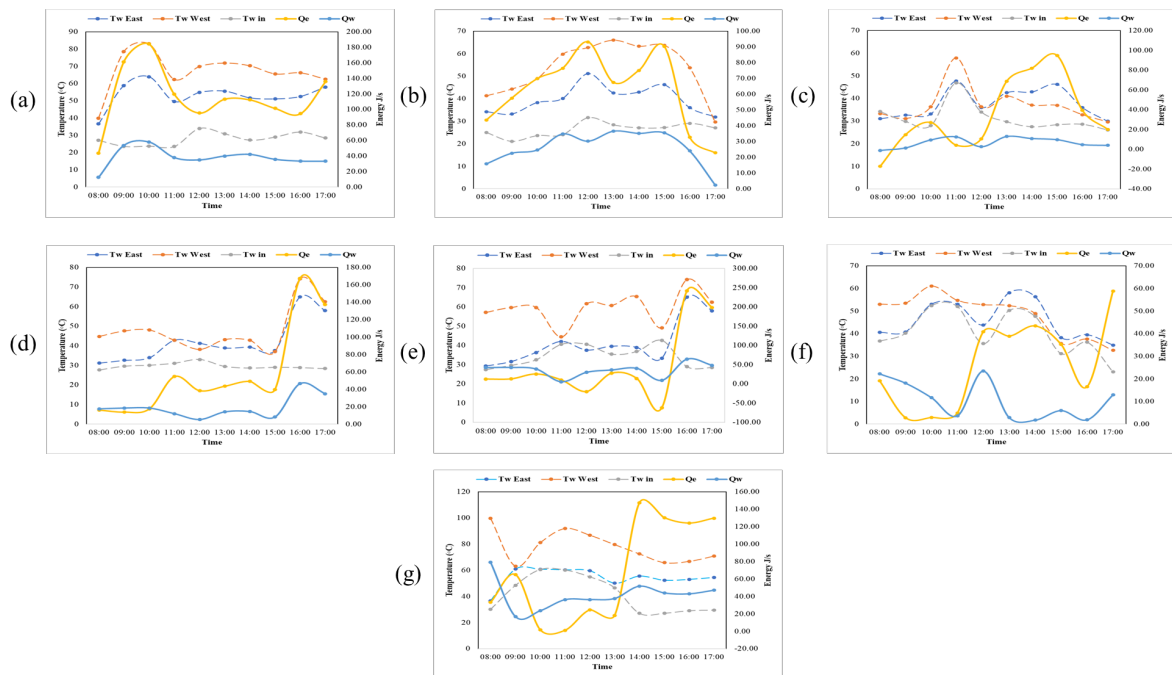


Fig. 20. Convection

Here,

Tw east = Water temperature inside the roof on the east side.

Tw west = Water temperature inside the roof on the west side.

Tw in = Water temperature entering the roof.

Qe = Heat on the east.

Qw = Heat on west

3.7.2.3 Radiation

Figure 21 illustrates the water temperature within the roof, ambient temperature, and total heat observed over the seven days. The chart indicates that the highest energy detected by the sensor peaked at 3 J/s between 11:00 - 12:00 WIB on the last day, while the lowest value was approximately 0 J/s at 17:00 WIB. The water temperature consistently exceeds the ambient temperature of 40°C to 90°C. In contrast, the ambient temperature remains relatively stable, ranging between 15°C to 30°C throughout the observation period.

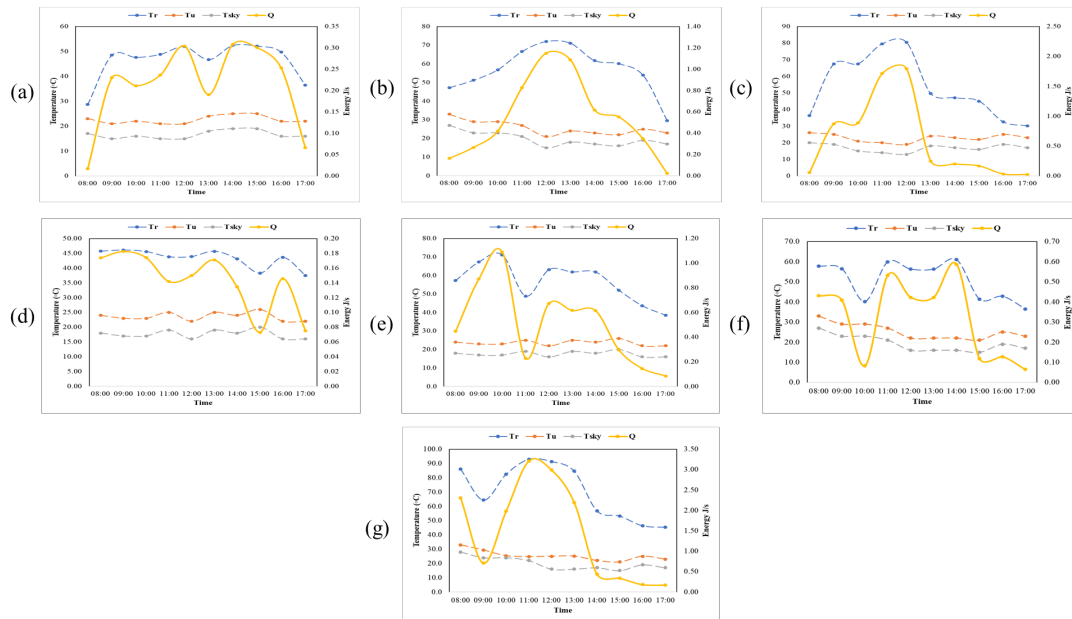


Fig. 21. Radiation

3.8 House 4 (Rice Husk and Fibreglass Material)

3.8.1 Heat temperature data

Figure 22 depicts the various temperatures recorded over the seven-day period, including water, inner and outer roof, and ambient temperatures. The temperature range commenced at 20°C, representing the lowest recorded water temperature entering the roofs. The highest temperature recorded was 120°C, observed within the water on both the eastern and western sides of the roofs.

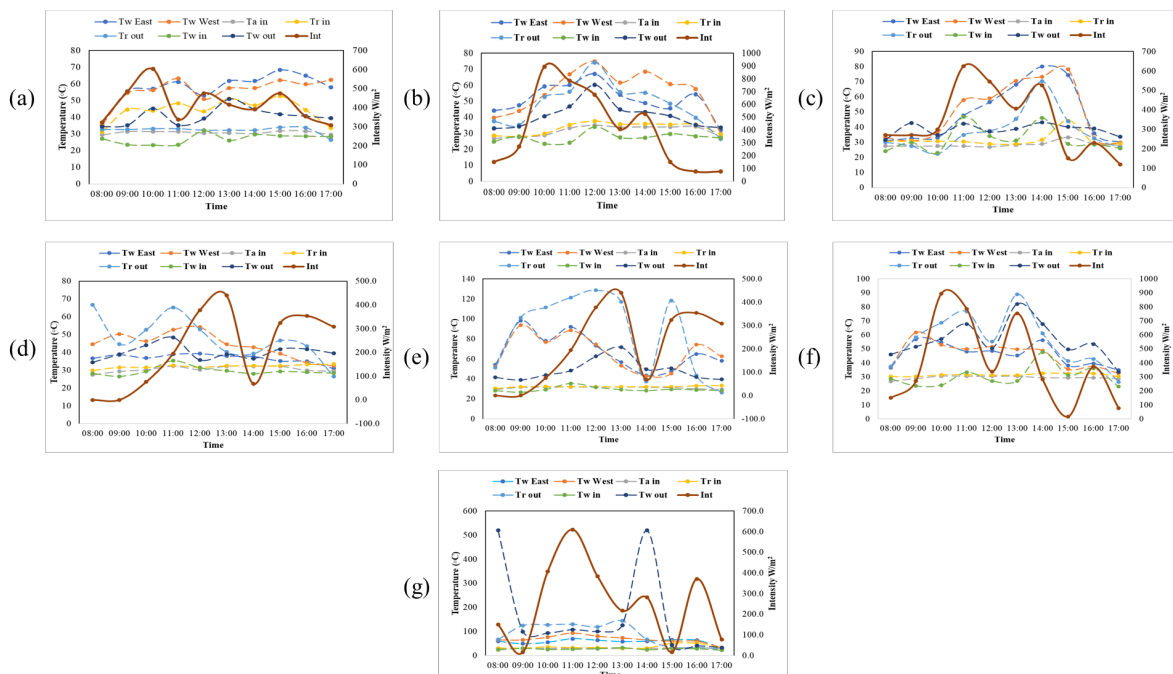


Fig. 22. The temperature data

Here,
 Tw east = Water temperature inside the roof on the east side.

- Tw west = Water temperature inside the roof on the west side.
- Ta in = Room temperature inside.
- Tr in = Inner roof surface temperature (east and west).
- Tr out = Outside roof surface temperature (east and west).
- Tw in = Water temperature entering the roof.
- Tw out = Water temperature coming out of the roof

3.8.2 Heat transfer rate

3.8.2.1 Conduction

Figure 23 illustrates the inner and outer roof surface temperatures and the total heat observed over seven days. The chart indicates that the highest energy detected by the sensor peaked at 400 J/s at 13:00 WIB on the last day, while the lowest value was approximately -70 J/s at 17:00 WIB. Regarding temperatures, the outer roof temperatures (both east and west) consistently exceed those of the inner roof, ranging between 70°C to 120°C, except on day one. Conversely, the inner roof temperature remains relatively stable, ranging between 30°C to 50°C throughout the observation period.

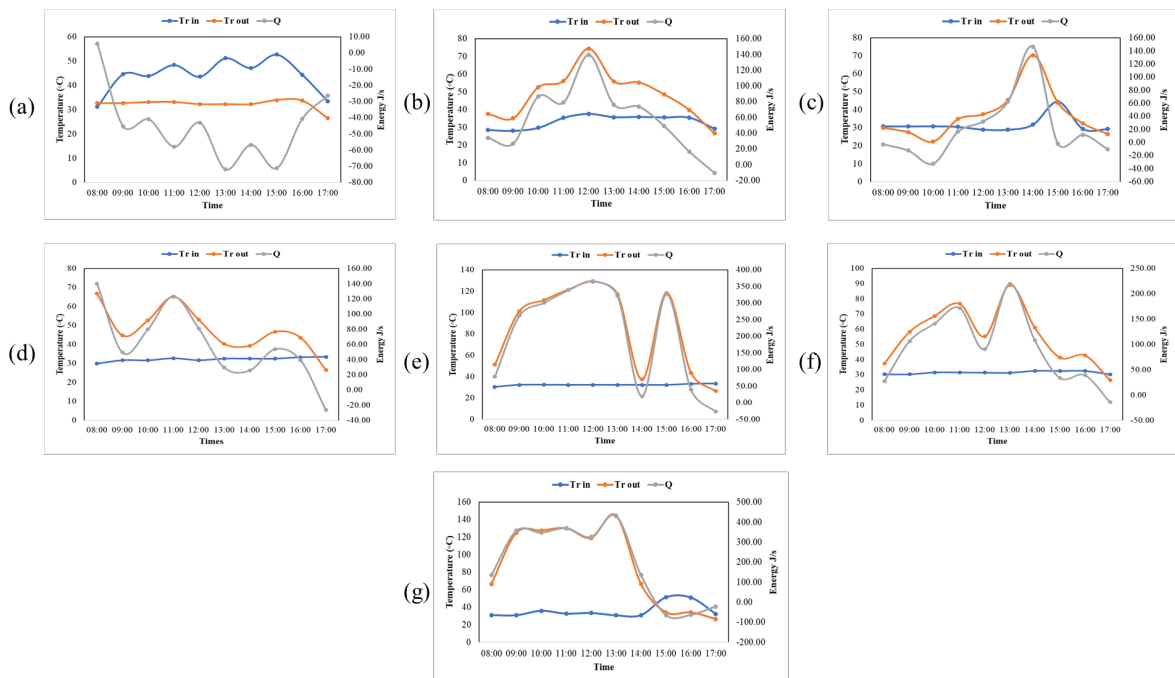


Fig. 23. Conduction

Here,

- Tr in = Inner roof surface temperature (east and west).
- Tr out = Outside roof surface temperature (east and west).
- Q = Total heat

3.8.2.2 Convection

Figure 24 presents the diverse temperatures recorded over the seven days, encompassing water temperatures inside the roof on the eastern and western sides, water temperature upon entry to the roof, and heat on the eastern and western sides of the roof. Throughout the observation period, the

heat on the western side consistently remains lower than on the eastern side, registering below 50 J/s. Conversely, the heat on the eastern side peaked at 250 J/s at 15:00 WIB on the sixth day. Regarding water temperatures, the temperature upon entry to the roof ranged between 20°C to 40°C, except on the third and sixth days when it reached 50°C at 11:00 WIB. Meanwhile, the inner roof temperature on both the eastern and western sides consistently remained higher, reaching 80°C. Additionally, the temperature on the western side peaked at 90 at 11:00 on the last day.

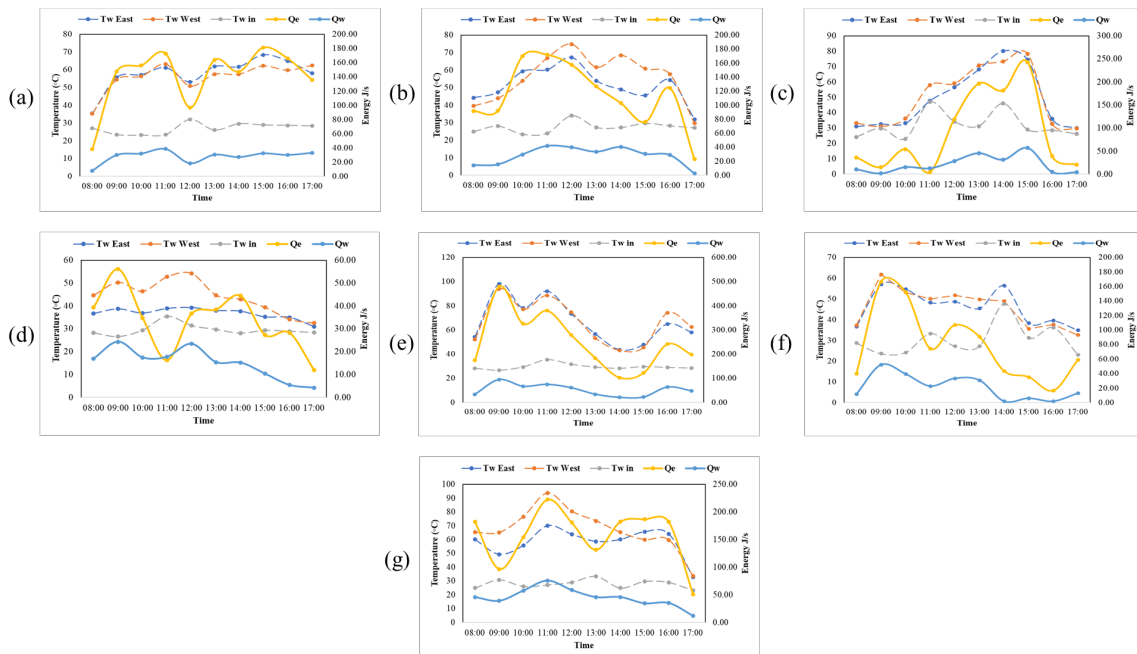


Fig. 24. Convection

Here,

- Tw east = Water temperature inside the roof on the east side.
- Tw west = Water temperature inside the roof on the west side.
- Tw in = Water temperature entering the roof.
- Qe = Heat on the east.
- Qw = Heat on the west.

3.8.2.3 Radiation

Figure 25 illustrates the water temperature within the roof, ambient temperature, and total heat across all seven days. Notably, the highest energy observed by the sensor peaked at 12 J/s at noon WIB on the fifth day, while the lowest energy was recorded at approximately 0 J/s at 17:00 WIB. The temperature data shows that the water temperature consistently exceeds the ambient temperature, ranging from 40°C to 120°C. In contrast, the ambient temperature remains relatively stable, ranging between 15°C to 30°C throughout the observation period.

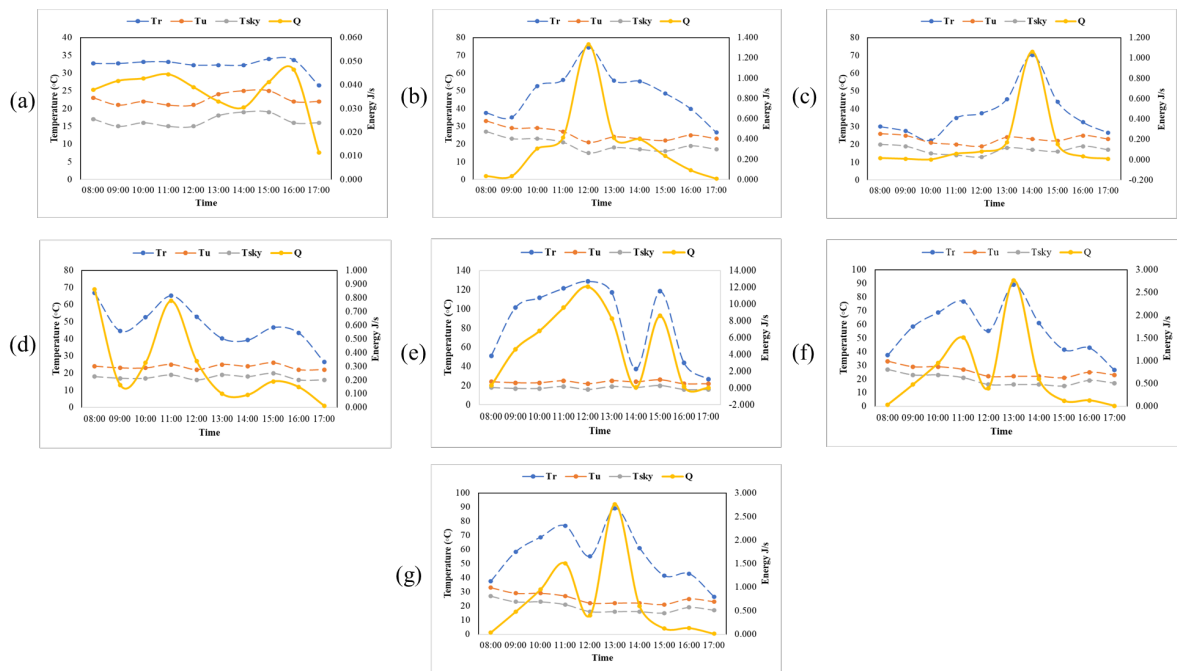


Fig. 25. Radiation

Here,

T_r = Water temperature inside the roof.

T_{sky} = Ambient temperature.

Q = Total heat

4. Conclusions

In conclusion, this study examined the performance and efficacy of composite layers applied to four distinct roof structures to identify the optimal composite layer among the options evaluated. Through a thorough analysis and assessment, Roof 2, comprising rice husk and wood fibre material, emerged as the superior choice.

Roof 2 exhibited exceptional attributes and advantages compared to the other roofs. Its composite layer demonstrated remarkable durability, excellent thermal insulation properties, and resilience against environmental stressors such as UV radiation and moisture. Moreover, Roof 2's composite layer displayed impressive heat-absorption capabilities, rendering it highly suitable for enduring harsh weather conditions. Additionally, it effectively mitigated heat transfer, leading to enhanced energy efficiency and reduced energy consumption within the building, aligning with sustainable construction practices.

Furthermore, Roof 2's composite layer's economic feasibility was evaluated, considering material costs, installation expenses, and maintenance requirements. The findings indicated that Roof 2 offered a balanced combination of cost-effectiveness and long-term performance, making it a financially viable option for residential and commercial settings.

In summary, after a comprehensive assessment of the four roof structures and their respective composite layers, Roof 2 emerged as the top choice. Its composite layer exhibited exceptional performance across various criteria, including durability, thermal insulation, environmental resistance, load-bearing capacity, energy efficiency, and economic feasibility. These findings offer valuable insights for architects, engineers, and construction professionals seeking the most suitable

composite layer for roof structures, underscoring Roof 2 as the preferred option for optimal performance, sustainability, and cost-effectiveness.

Acknowledgement

This research was not funded by any grant.

References

- [1] Zhong, Yetao, Zhen Fang, Boyu Cao, Shigang Wu, Xiaochun Fan, and Zhilin Xia. "An adaptive direct evaporative cooler that regulates the sub-ambient temperature by controlling the evaporation rate." *Journal of Thermal Science and Engineering Applications* 15, no. 5 (2023): 051004. <https://doi.org/10.1115/1.4056978>
- [2] Daud, Mohamad Khairul Aiman, Ili Najaa Aimi Mohd Nordin, Tuan Noor Hasanah Tuan Ismail, Effendy Adam, Noraishikin Zulkarnain, Muhammad Rusydi Muhammad Razif, and Tariq Rehman. "Development of Smart Chopper Composting Monitoring System." *Journal of Advanced Research in Applied Sciences and Engineering Technology* 42, no. 2 (2024): 197-208. <https://doi.org/10.37934/araset.42.2.197208>
- [3] Change, IPCC Climate. "The science of climate change." *Second Assessment Report of the Intergovernmental Panel on Climate Change*. Cambridge University Press, Cambridge (1996).
- [4] Azemi, Nur Liesa Mohammad, Munirah Mohd Yusof, Hanayanti Hafit, Aeslina Abdul Kadir, and Mohamad Aizi Salamat. "Design and Development of A Web-Based Smart Recycling System based on a Survey on Recycling Awareness." *Journal of Advanced Research in Applied Sciences and Engineering Technology* 41, no. 2 (2024): 180-193. <https://doi.org/10.37934/araset.41.2.180193>
- [5] Coulomb, Didier. "Environmental Issues Related to Refrigeration Technologies." *International Journal of Air-Conditioning and Refrigeration* 29, no. 02 (2021): 2130002. <https://doi.org/10.1142/S2010132521300020>
- [6] Lin, Lee Yee, Khoo Terh Jing, Chai Tze Qing, and Ha Chin Yee. "Sustainable Development in Renewable Energy: Management of Solar Energy Application in Malaysia." *Journal of Advanced Research in Applied Sciences and Engineering Technology* 43, no. 1 (2025): 1-16. <https://doi.org/10.37934/araset.43.1.116>
- [7] Yu, Meng, and Zhiyun Zou. "Design of structure and control system of semiconductor refrigeration box." *Chinese Journal of Chemical Engineering* 28, no. 11 (2020): 2792-2798. <https://doi.org/10.1016/j.cjche.2020.07.035>
- [8] Ahamed, Jamal Uddin, Rahman Saidur, and Haji Hassan Masjuki. "A review on exergy analysis of vapor compression refrigeration system." *Renewable and Sustainable Energy Reviews* 15, no. 3 (2011): 1593-1600. <https://doi.org/10.1016/j.rser.2010.11.039>
- [9] Tarbutt, M. R. "Laser cooling of molecules." *Contemporary Physics* (2019).
- [10] Jang, Dongjin, Thomas Gruner, Alexander Steppke, Keisuke Mitsumoto, Christoph Geibel, and Manuel Brando. "Large magnetocaloric effect and adiabatic demagnetization refrigeration with YbPt2Sn." *Nature communications* 6, no. 1 (2015): 8680. <https://doi.org/10.1038/ncomms9680>
- [11] Cui, Shuang, Chihyung Ahn, Matthew C. Wingert, David Leung, Shengqiang Cai, and Renkun Chen. "Bio-inspired effective and regenerable building cooling using tough hydrogels." *Applied energy* 168 (2016): 332-339. <https://doi.org/10.1016/j.apenergy.2016.01.058>
- [12] Berardi, Umberto, Massimo Garai, and Thomas Morselli. "Preparation and assessment of the potential energy savings of thermochromic and cool coatings considering inter-building effects." *Solar Energy* 209 (2020): 493-504. <https://doi.org/10.1016/j.solener.2020.09.015>
- [13] Giamasrow, Rudraa Devi, Nurhafizah Abu Talip Yusof, Azahani Natasha Azman, Norazwina Zainol, and Mohamad Shaiful Abdul Karim. "Fabrication of Cellulose Powder Dielectric Composite Material using Pineapple Leaves Fiber." *Journal of Advanced Research in Applied Sciences and Engineering Technology* 38, no. 2 (2024): 1-15. <https://doi.org/10.37934/araset.38.2.115>
- [14] Zhou, Hongyu, and Adam L. Brooks. "Thermal and mechanical properties of structural lightweight concrete containing lightweight aggregates and fly-ash cenospheres." *Construction and Building Materials* 198 (2019): 512-526. <https://doi.org/10.1016/j.conbuildmat.2018.11.074>
- [15] Brooks, Adam L., Hongyu Zhou, and Dominic Hanna. "Comparative study of the mechanical and thermal properties of lightweight cementitious composites." *Construction and Building Materials* 159 (2018): 316-328. <https://doi.org/10.1016/j.conbuildmat.2017.10.102>
- [16] Alias, Nur Nazira, Ireana Yusra Abdul Fatah, Yew Been Seok, Sharifah Hanis Yasmin Sayid Abdullah, Amir Hussain Bhat, and Saiful Bahri Mohd Diah. "Material Characterizations of the Polymers Reinforced with Recycled Flexible Plastic Blends as Filament for 3D Printing." *Journal of Advanced Research in Applied Sciences and Engineering Technology* 37, no. 1 (2024): 1-15. <https://doi.org/10.37934/araset.37.1.115>

- [17] Zhou, Tingjiao, Jinbin Yang, Deyong Zhu, Jieyao Zheng, Stephan Handschuh-Wang, Xiaohu Zhou, Junmin Zhang et al., "Hydrophilic sponges for leaf-inspired continuous pumping of liquids." *Advanced Science* 4, no. 6 (2017): 1700028. <https://doi.org/10.1002/advs.201700028>
- [18] Salehoh, Muhammad Mahfuz, Zul Izie Hafifi Mohamad Ghazali, Ahmad Nazirul Manan, Nur Farahana Mat Isa, Nur Aisyah Mohd Yusri, Hafizal Yahaya, Rasli Abd Ghani, and Fauzan Ahmad. "The Effect of an Aluminium Disc Rotator on Polyvinyl Chloride (PVC) Material using 360° Lateral Sliding Disc Triboelectric Generator (TEG)." *Journal of Advanced Research in Applied Sciences and Engineering Technology* 34, no. 1 (2024): 187-198. <https://doi.org/10.37934/araset.34.1.187198>
- [19] Kuehni, Salomé MS Shokri, Elie Bou-Zeid, Colin Webb, and Nima Shokri. "Roof cooling by direct evaporation from a porous layer." *Energy and Buildings* 127 (2016): 521-528. <https://doi.org/10.1016/j.enbuild.2016.06.019>
- [20] Admoko, Davin Arkan, Bambang Darmawan, A. Ana, and Vina Dwiyantri. "A Cluster-Based Bibliometric Analysis of the Emerging Technological Landscape in Logistics using Vosviewer." *Journal of Advanced Research in Applied Sciences and Engineering Technology* 42, no. 2 (2024): 234-249. <https://doi.org/10.37934/araset.42.2.234249>
- [21] Sazali, Norsuhailizah, Zawati Harun, and Norazlianie Sazali. "Additional of Organic Amendments in the Soil to Increase the Various Crop Yield: A Review." *Journal of Advanced Research in Applied Sciences and Engineering Technology* 35, no. 2 (2024): 158-174. <https://doi.org/10.37934/araset.35.2.158174>
- [22] Ascione, Fabrizio. "Energy conservation and renewable technologies for buildings to face the impact of the climate change and minimize the use of cooling." *Solar Energy* 154 (2017): 34-100. <https://doi.org/10.1016/j.solener.2017.01.022>
- [23] Jacob, Daniela, Lola Kotova, Claas Teichmann, Stefan P. Sobolowski, Robert Vautard, Chantal Donnelly, Aristeidis G. Koutroulis et al., "Climate impacts in Europe under+ 1.5 C global warming." *Earth's Future* 6, no. 2 (2018): 264-285. <https://doi.org/10.1002/2017EF000710>
- [24] Santamouris, Mat. "Cooling the buildings—past, present and future." *Energy and Buildings* 128 (2016): 617-638. <https://doi.org/10.1016/j.enbuild.2016.07.034>
- [25] Kaboré, Madi, Emmanuel Bozonnet, Patrick Salagnac, and Marc Abadie. "Indexes for passive building design in urban context—indoor and outdoor cooling potentials." *Energy and Buildings* 173 (2018): 315-325. <https://doi.org/10.1016/j.enbuild.2018.05.043>
- [26] Davis, Ryan, Troy R. Hawkins, Andre Coleman, Song Gao, Bruno Klein, Matthew Wiatrowski, Yunhua Zhu et al., *Economic, Greenhouse Gas, and Resource Assessment for Fuel and Protein Production from Microalgae: 2022 Algae Harmonization Update*. No. NREL/TP-5100-87099. National Renewable Energy Laboratory (NREL), Golden, CO (United States), 2024. <https://doi.org/10.2172/2318964>
- [27] Karim, Malik Abdul, Mohamad Zaki Abdullah, Ahmed Farouk Deifalla, Marc Azab, and Ahsan Waqar. "An assessment of the processing parameters and application of fibre-reinforced polymers (FRPs) in the petroleum and natural gas industries: A review." *Results in Engineering* (2023): 101091. <https://doi.org/10.1016/j.rineng.2023.101091>
- [28] Karim, M., M. Abdullah, and Tauseef Ahmed. "AN overview: the processing methods of fiber-reinforced polymers (FRPS)." *J. Mech. Eng. Technol* 12 (2021): 10-24. <https://doi.org/10.34218/IJMET.12.2.2021.002>
- [29] Karim, Malik Abdul, Mohamad Zaki Abdullah, Ahsan Waqar, Ahmed Farouk Deifalla, Adham E. Ragab, and Muhammad Khan. "Analysis of the mechanical properties of the single layered braid reinforced thermoplastic pipe (BRTP) for oil & gas industries." *Results in Engineering* 20 (2023): 101483. <https://doi.org/10.1016/j.rineng.2023.101483>
- [30] Huang, Rui, Jinxin Feng, Ziyue Ling, Xiaoming Fang, and Zhengguo Zhang. "A sodium acetate trihydrate-formamide/expanded perlite composite with high latent heat and suitable phase change temperatures for use in building roof." *Construction and Building Materials* 226 (2019): 859-867. <https://doi.org/10.1016/j.conbuildmat.2019.07.331>
- [31] Chang, Seong Jin, Seunghwan Wi, Hyun Mi Cho, Su-Gwang Jeong, and Sumin Kim. "Numerical analysis of phase change materials/wood–plastic composite roof module system for improving thermal performance." *Journal of Industrial and Engineering Chemistry* 82 (2020): 413-423. <https://doi.org/10.1016/j.jiec.2019.11.005>
- [32] Ghosh, Arghya, and Dipankar Chakravorty. "Failure analysis of civil engineering composite shell roofs." *Procedia engineering* 173 (2017): 1642-1649. <https://doi.org/10.1016/j.proeng.2016.12.258>
- [33] Neogi, Sanjoy Das, Amit Karmakar, and Dipankar Chakravorty. "Finite element analysis of laminated composite skewed hypar shell roof under oblique impact with friction." *Procedia engineering* 173 (2017): 314-322. <https://doi.org/10.1016/j.proeng.2016.12.023>
- [34] Irawati, Inggar Septhia, Ali Awaludin, and Nicholas Padua Sebastian. "The performance of cold-formed steel long-span roof structure combined with laminated timber: Cold-formed steel–laminated timber composite." *Procedia engineering* 171 (2017): 1242-1249. <https://doi.org/10.1016/j.proeng.2017.01.417>

- [35] Ong, Kok Seng. "Temperature reduction in attic and ceiling via insulation of several passive roof designs." *Energy Conversion and Management* 52, no. 6 (2011): 2405-2411. <https://doi.org/10.1016/j.enconman.2010.12.044>
- [36] Khalifa, A. H. N. "Effect of roof pond on the energy and exergy performance of a single space building." *Journal of Thermal Engineering* 3, no. 3 (2017): 1275-1293. <https://doi.org/10.18186/journal-of-thermal-engineering.323394>
- [37] Kong, Xiangfei, Shilei Lu, Yiran Li, Jingyu Huang, and Shangbao Liu. "Numerical study on the thermal performance of building wall and roof incorporating phase change material panel for passive cooling application." *Energy and Buildings* 81 (2014): 404-415. <https://doi.org/10.1016/j.enbuild.2014.06.044>
- [38] Kumar, Ashok, and B. M. Suman. "Experimental evaluation of insulation materials for walls and roofs and their impact on indoor thermal comfort under composite climate." *Building and environment* 59 (2013): 635-643. <https://doi.org/10.1016/j.buildenv.2012.09.023>
- [39] Al-Obaidi, Karam M., Mazran Ismail, and Abdul Malek Abdul Rahman. "Passive cooling techniques through reflective and radiative roofs in tropical houses in Southeast Asia: A literature review." *Frontiers of Architectural Research* 3, no. 3 (2014): 283-297. <https://doi.org/10.1016/j.foar.2014.06.002>
- [40] Abdulhamed, A. J. "Design and analysis of medium scale water production using solar parabolic trough collector with turbulator baffles." PhD diss., Ph. D. Thesis. Faculty of engineering, University Putra Malaysia, Malaysia, Selangor, 2018.
- [41] Dobriyal, Ritvik, Prateek Negi, Neeraj Sengar, and Desh Bandhu Singh. "A brief review on solar flat plate collector by incorporating the effect of nanofluid." *Materials today: proceedings* 21 (2020): 1653-1658. <https://doi.org/10.1016/j.matpr.2019.11.294>
- [42] Deng, Jie, Tadhg S. O'Donovan, Zhiyong Tian, Josh King, and Stuart Speake. "Thermal performance predictions and tests of a novel type of flat plate solar thermal collectors by integrating with a freeze tolerance solution." *Energy conversion and management* 198 (2019): 111784. <https://doi.org/10.1016/j.enconman.2019.111784>
- [43] Kumar, Suresh, and S. C. Mullick. "Wind heat transfer coefficient in solar collectors in outdoor conditions." *Solar energy* 84, no. 6 (2010): 956-963. <https://doi.org/10.1016/j.solener.2010.03.003>
- [44] H. L. Penman and P. A. Sheppard, "Radiation Skies," (1964): 488-493.
- [45] M. H. and A. E.-H. M.S.El-Sebaey, Sh. Shams El-Din. "Effect of External Reflector Angle on Productivity and Performance of Double Slope Solar Still with Internal Parabolic Reflector," *IOSR Journal of Mechanical Civil Engineering*, vol. 9, no. 6, (2013): 40-54. <https://doi.org/10.9790/1684-0964054>
- [46] Tiwari, G. N., and Lovedeep Sahota. "Review on the energy and economic efficiencies of passive and active solar distillation systems." *Desalination* 401 (2017): 151-179. <https://doi.org/10.1016/j.desal.2016.08.023>
- [47] Sahota, Lovedeep, and G. N. Tiwari. "Energy matrices, enviroeconomic and exergoeconomic analysis of passive double slope solar still with water based nanofluids." *Desalination* 409 (2017): 66-79. <https://doi.org/10.1016/j.desal.2017.01.012>
- [48] Damanik, Wawan Septiawan, Farel H. Napitupulu, A. Halim Nasution, and Himsar Ambarita. "Energy analysis of double slope aktive solar still." In *IOP Conference Series: Materials Science and Engineering*, vol. 725, no. 1, p. 012007. IOP Publishing, 2020. <https://doi.org/10.1088/1757-899X/725/1/012007>
- [49] Majumdar, Rudrodip, Sandip K. Saha, and Aditya Patki. "Novel dimension scaling for optimal mass flow rate estimation in low temperature flat plate solar collector based on thermal performance parameters." *Thermal Science and Engineering Progress* 19 (2020): 100569. <https://doi.org/10.1016/j.tsep.2020.100569>
- [50] Gao, Datong, Guangtao Gao, Jingyu Cao, Shuai Zhong, Xiao Ren, Yousef N. Dabwan, Maobin Hu, Dongsheng Jiao, Trevor Hocksun Kwan, and Gang Pei. "Experimental and numerical analysis of an efficiently optimized evacuated flat plate solar collector under medium temperature." *Applied Energy* 269 (2020): 115129. <https://doi.org/10.1016/j.apenergy.2020.115129>